2018 European Control Conference (ECC)
June 12-15, 2018. Limassol, Cyprus

Point-to-Point Repetitive Control with Application to Drop-Foot

A. P. Page, C. T. Freeman and B. Chu

Abstract— **Drop-foot is characterised by ankle dorsiflexion weakness, caused by either nerve damage or a result of a brain or spinal injury. It results in abnormal gait, producing slow, tiring and often unsafe ambulation. Established treatment is via passive orthoses, but these have high rejection rates caused by discomfort, loss of muscle control and ankle instability. Functional electrical stimulation (FES) has had considerable success, but current commercial control approaches are open loop or triggered, and the few exisiting feedback approaches require extensive sensor data, lack accuracy, or are highly dependent on an identified model. This paper is the first application of repetitive control (RC) to this problem, providing improved gait performance by learning from errors over previous gait cycles. To address the drawbacks of previous approaches, a comprehensive extension to a general class of RC law is developed which enables it to track only isolated time points. Simulation results of the resulting 'point-to-point' RC framework on FES-assisted drop-foot confirm its improved convergence and robust performance properties.**

I. INTRODUCTION

Drop-foot is a common problem resulting from a range of neurological conditions, and prevents normal leg swing during gait, leading to abnormal, inefficient motion and increased risk of falling. Typically caused by compression or damage to the peroneal nerve, it manifests in 20% of people who have experienced a stroke [1]. Multiple sclerosis (MS) can also lead to Drop-Foot, with studies showing that 63% of people with MS fear falling and 83% thus avoiding activity [2]. Full recovery from Drop-Foot if due to skeletal or neuropathy/neurological issues is not possible, hence the need for effective technologies to aid mobility is substantial.

Current approaches have demonstrated significant improvements in gait quality, usually measured in terms of speed, reduction of effort and decreased feelings of anxiety and depression. However significant limitations remain in terms of both performance and usability. The most established interventions comprise mechanical ankle orthoses, however these typically restrict motion and can discourage recovery, leading to increased spasticity and soft tissue shortening. For this reason, clinicians are often unwilling to prescribe such devices, as reflected by studies in which 47% have never used them [3]. Even when used, rejection rates of 30% are typical, with a negative effect upon dignity cited as a primary limitation. Functional electrical stimulation (FES) involves artificial activation of the peroneal nerve, and is the leading active intervention technology. FES has been shown to produce improved walking gait cycles in patients as well as being smaller and a more controllable solution than mechanical systems. Clinical trials of FES have shown an increase in walking speed by 16%, a reduction in effort of 29% as well as reduced spasticity, anxiety and depression [4]. Additional research shows FES provides long term recovery benefits [5]: sit to stand is easier due to reduced compensatory motion and improved knee/hip flexion.

All commercial systems employ open-loop FES, usually triggered by a pressure sensor mounted in the heel, producing crude assistance in dorsiflexion around the ankle. More advanced controllers have been developed to provide more natural motion. For example an iterative learning control (ILC) algorithm was proposed using run-to-run control of the maximum foot pitch angle which occurred during a patient walking [6]. Previously to this, similar results were obtained through the use of a bend sensor and a fuzzy logic algorithm [7]. However, both these systems used simplifed dynamics and provided limited accuracy. An innovative approach used ILC with variable pass length in [8], employing 6 inertial measurements to track the entire pitch angle trajectory. Although effective this requires significant sensor data, an accurate system model, and is based on the ILC assumption that the system resets to a fixed state at the start of each trial (which does not strictly hold for gait).

This paper addresses these drawbacks by developing the first repetitive control (RC) implementation for Drop-Foot. This first requires a substantial extension to the underlying RC framework, since existing RC schemes either enforce tracking at all time points or over predefined frequencies [9]. This paper develops 'point-to-point' RC which only enforces tracking at a subset of points specified by the designer (e.g. at a minimal set of points which define the task). This is a translation of a similar ILC concept which has been shown to provide greater robustness to plant uncertainty [10].

II. POINT-TO-POINT RC FORMULATION

Let P denote the LTI discrete-time dynamics given by minimal state-space system (A_P, B_P, C_P, D_P) where

$$P:\ u \mapsto y\ :\begin{cases} x_P(i+1) = A_P x_P(i) + B_P u(i) \\ y(i) = C_P x_P(i) + D_P u(i), \end{cases} \tag{1}$$

with $A_P \in \mathbb{R}^{n_P \times n_P}$, $B_P \in \mathbb{R}^{n_P \times m}$, $C_P \in \mathbb{R}^{o \times n_P}$ and $D_P \in \mathbb{R}^{o \times m}$. In the standard RC framework it is assumed that an N-periodic reference r is defined by the designer, i.e. $r(i) = r(i+N)$ for a given $N \in \mathbb{N}$ and all $i \in \mathbb{N}$. The tracking problem is then to achieve asymptotic convergence of the system output to the reference, that is for $k \in \mathbb{N}$

$$\lim_{k\to\infty} y(kN+i) = r(i), \quad i = 0, \cdots, N-1 \tag{2}$$

The authors are with Electronics and Computer Science, University of Southampton, Southampton, SO17 1BJ, UK {app2g13,cf,bc}@soton.ac.uk

while the control input similarly converges to a limit, $\hat{u}$, as

$$\lim_{k\to\infty} u(kN+i) = \hat{u}(i), \quad i = 0, \cdots, N-1. \tag{3}$$

RC design is typically conducted using the one-sample advance operator q, defined by $q(v(k)) = v(k+1)$ for any $v \in \mathcal{L}_2^r$. The most common form of RC update algorithm is

$$u(i+N) = Q(q)(u(i) + L(q)e(i)), \;\; u(-i) = 0 \; \forall \, i \in \mathbb{N} \tag{4}$$

where $e = r - y$ is the tracking error, and $Q(q)$, $L(q)$ are filters to be designed. From (4) it follows that the disturbance-free control action evolution is

$$u(i+N) = Q(q)(I - L(q)P(q))u(i) + Q(q)L(q)r(i) \tag{5}$$

where $P(q) = C_P(Iq - A_P)^{-1}B_P + D_P$. The overall controller must be causal, which constrains design of $Q(q)$ and $L(q)$ which are both typically non-causal. A necessary and sufficient condition for convergence is that the roots of

$$1 - q^{-N}Q(q)(1 - P(q)L(q)) = 0 \tag{6}$$

all lie inside the unit circle. A sufficient condition is

$$\|Q(q)(1 - P(q)L(q))\|_\infty < 1 \tag{7}$$

or equivalently, in the frequency domain by

$$\sup_{\omega\in[0,\pi]} |Q(e^{j\omega})(1 - P(e^{j\omega})L(e^{j\omega}))| < 1. \tag{8}$$

For arbitrary r, convergence to zero error requires $Q(q) = I$.

III. LIFTED RC FORMULATION

The development of point-to-point RC requires the lifted framework defined using the signals

$$\begin{aligned}\boldsymbol{u}(k) =& [u(kN), u(kN+1), \cdots u((k+1)N-1)]^\top \in \mathbb{R}^{mN},\\ \boldsymbol{y}(k) =& [y(kN), y(kN+1), \cdots y((k+1)N-1)]^\top \in \mathbb{R}^{oN},\end{aligned}$$

for $k \in \mathbb{N}$, together with

$$\begin{aligned}\boldsymbol{r}(k) = \boldsymbol{r} &= [r(0),\; r(1), \cdots r(N-1)]^\top \in \mathbb{R}^{oN}, \quad (9)\\ \boldsymbol{e}(k) &= \boldsymbol{r} - \boldsymbol{y}(k) \in \mathbb{R}^{oN}. \quad (10)\end{aligned}$$

The tracking requirement (2) equivalently becomes

$$\lim_{k\to\infty} \boldsymbol{y}(k) = \boldsymbol{r} \tag{11}$$

and lifted update (4) can similarly be written as

$$\boldsymbol{u}(k+1) = \boldsymbol{Q}(\boldsymbol{q})\big(\boldsymbol{u}(k) + \boldsymbol{L}(\boldsymbol{q})\boldsymbol{e}(k)\big) \tag{12}$$

The plant dynamics can therefore be equivalently expressed by the state-space system

$$\boldsymbol{P}: \begin{cases} \underbrace{x_P((k+1)N)}_{\boldsymbol{x}_P(k+1)} = \underbrace{A_P^N}_{\boldsymbol{A}_P}\underbrace{x_p(kN)}_{\boldsymbol{x}_P(k)} + \\ \qquad \underbrace{[A_P^{N-1}B_P,\; A_P^{N-2}B_P, \cdots B_P]}_{\boldsymbol{B}_P}\boldsymbol{u}(k) \\ \boldsymbol{y}(k) = \underbrace{\begin{bmatrix} C_P \\ C_PA_P \\ \vdots \\ C_PA_P^{N-1}\end{bmatrix}}_{\boldsymbol{C}_P}\underbrace{x_P(kN)}_{\boldsymbol{x}_P(k)} + \\ \qquad \underbrace{\begin{bmatrix} D_P & 0 & \cdots & 0 \\ C_PB_P & D_P & \ddots & \vdots \\ \vdots & \ddots & \ddots & 0 \\ C_PA_P^{N-2}B_P \cdots & C_PB_P & D_P\end{bmatrix}}_{\boldsymbol{D}_P}\boldsymbol{u}(k) \end{cases} \tag{13}$$

where $\boldsymbol{A}_P \in \mathbb{R}^{n_P\times n_P}$, $\boldsymbol{B}_P \in \mathbb{R}^{n_P\times mN}$, $\boldsymbol{C}_P \in \mathbb{R}^{oN\times n_P}$ and $\boldsymbol{D}_P \in \mathbb{R}^{oN\times mN}$. Assuming no specific structure, we can also define lifted forms of $\boldsymbol{Q}(\boldsymbol{q})$ and $\boldsymbol{L}(\boldsymbol{q})$ as

$$\boldsymbol{Q}: \begin{cases} \boldsymbol{x}_Q(k+1) \;=\; \boldsymbol{A}_Q\boldsymbol{x}_Q(k) + \boldsymbol{B}_Q(\boldsymbol{v}+\boldsymbol{u})(k) \\ \boldsymbol{u}(k+1) \;=\; \boldsymbol{C}_Q\boldsymbol{x}_Q(k) + \boldsymbol{D}_Q(\boldsymbol{v}+\boldsymbol{u})(k) \end{cases} \tag{14}$$

where $\boldsymbol{A}_Q \in \mathbb{R}^{n_Q\times n_Q}$, $\boldsymbol{B}_Q \in \mathbb{R}^{n_Q\times mN}$, $\boldsymbol{C}_Q \in \mathbb{R}^{mN\times n_Q}$ and $\boldsymbol{D}_Q \in \mathbb{R}^{mN\times mN}$. Finally we have

$$\boldsymbol{L}: \begin{cases} \boldsymbol{x}_L(k+1) \;=\; \boldsymbol{A}_L\boldsymbol{x}_L(k) + \boldsymbol{B}_L\boldsymbol{e}(k) \\ \boldsymbol{v}(k) \;=\; \boldsymbol{C}_L\boldsymbol{x}_L(k) + \boldsymbol{D}_L\boldsymbol{e}(k) \end{cases} \tag{15}$$

where $\boldsymbol{A}_L \in \mathbb{R}^{n_L\times n_L}$, $\boldsymbol{B}_L \in \mathbb{R}^{n_L\times oN}$, $\boldsymbol{C}_L \in \mathbb{R}^{mN\times n_L}$ and $\boldsymbol{D}_L \in \mathbb{R}^{mN\times oN}$. More structured forms of (14) and (15) can be given if $Q(q)$ and $L(q)$ have explicit unlifted state-space forms (see [11]). Convergence condition (25) expressed for the lifted system corresponds to

$$\|\boldsymbol{Q}(\boldsymbol{q})(1 - \boldsymbol{P}(\boldsymbol{q})\boldsymbol{L}(\boldsymbol{q}))\|_\infty < 1 \tag{16}$$

and it is shown in [11] that (25) implies (16).

A. Point-to-point RC

Suppose it is only necessary to track a subset of $M < N$ points of reference $\boldsymbol{r}$, with indices

$$i = i_1, i_2, \cdots, i_M \tag{17}$$

which can be extracted from $\boldsymbol{r}$ using the projection operator $\boldsymbol{\Phi}: \mathcal{L}^{mN} \to \mathcal{L}^{mM}$. For any lifted signal $\boldsymbol{s} \in \mathcal{L}^{mN}$, define

$$\boldsymbol{\Phi}\colon \mathcal{L}^{mN} \to \mathcal{L}^{mM}\colon \boldsymbol{s} \mapsto \boldsymbol{s}^\Phi\colon \boldsymbol{s}^\Phi(i) = \begin{bmatrix} s(iN+i_1) \\ s(iN+i_2) \\ \vdots \\ s(iN+i_M)\end{bmatrix} = \bar{\Phi}\boldsymbol{s}(i) \tag{18}$$

where $\bar{\Phi}\boldsymbol{s}(i) \in \mathbb{R}^{mM}$ and

$$\bar{\Phi}_{j,i} = \begin{cases} I, & \text{if} \quad i = i_j \\ 0, & \text{otherwise} \end{cases} \tag{19}$$

In particular the set of point-to-point output positions are

$$\boldsymbol{r}^\Phi = \bar{\Phi}\boldsymbol{r} = \begin{bmatrix} r(i_1),\; r(i_2),\; \cdots \;\; r(i_M) \end{bmatrix}^\top. \tag{20}$$

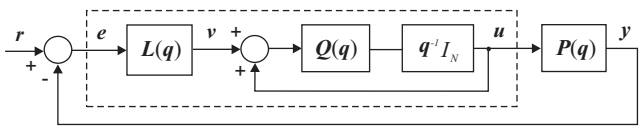

Fig. 1. RC system lifted description.

We use this to replace $\boldsymbol{r}$ by $\boldsymbol{\Phi r} = \boldsymbol{r}^{\Phi}$ and $\boldsymbol{e}$ by $\boldsymbol{\Phi e} = \boldsymbol{e}^{\Phi}$ in the standard RC framework, where $\boldsymbol{Q}(\boldsymbol{q})$ and $\boldsymbol{L}(\boldsymbol{q})$ must be redesigned for this lower dimensional system. The new system is shown in Fig. 2. and objective (11) is replaced

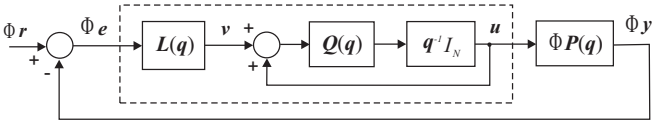

Fig. 2. Point-to-point RC system lifted description.

by

$$\lim_{k\to\infty} \boldsymbol{y}^{\Phi}(k) = \boldsymbol{r}^{\Phi} \tag{21}$$

and (3) is replaced in lifted form by

$$\lim_{k\to\infty} \boldsymbol{u}(k) = \hat{\boldsymbol{u}} \tag{22}$$

It is now possible to state the following result.

Theorem 1: The lifted update

$$\boldsymbol{u}(k+1) = \boldsymbol{u}(k) + \boldsymbol{L}(\boldsymbol{q})\boldsymbol{e}^{\Phi}(k) \tag{23}$$

applied to system (13) where $\boldsymbol{e}^{\Phi}(k) = \boldsymbol{r}^{\Phi} - \boldsymbol{\Phi y}(k)$, and $\boldsymbol{L}(\boldsymbol{q}) : \mathcal{L}^{mM} \to \mathcal{L}^{mN}$ is selected to satisfy

$$\|I - \boldsymbol{\Phi P}(\boldsymbol{q})\boldsymbol{L}(\boldsymbol{q})\|_{\infty} < 1 \tag{24}$$

solves the point-to-point RC problem (21).

Proof: Follows by exploiting the dimensional freedom available in the lifted convergence analysis, see e.g. [11]. ■

Next consider design of a suitable filter $\boldsymbol{L}(\boldsymbol{q})$ to satisfy (24).

Theorem 2: Suppose unlifted operator $\bar{L}(q)$ is designed to satisfy the traditional RC criterion

$$\|I - P(q)\bar{L}(q)\|_{\infty} < 1 \tag{25}$$

or alternatively, in the frequency domain

$$\sup_{\omega\in[0,\pi]} |I - P(e^{j\omega})\bar{L}(e^{j\omega})| < 1 \tag{26}$$

then the operator

$$\boldsymbol{L}(\boldsymbol{q}) = \bar{\boldsymbol{L}}(\boldsymbol{q})\boldsymbol{\Phi}^{*} \tag{27}$$

satisfies condition (24) where $(\cdot)^{*}$ is the adjoint operator.

Proof: Insert form (27) into (24) gives

$$\|I - \boldsymbol{\Phi P}(\boldsymbol{q})\bar{\boldsymbol{L}}(\boldsymbol{q})\boldsymbol{\Phi}^{*}\|_{\infty} = \|\boldsymbol{\Phi}\big(I - \boldsymbol{P}(\boldsymbol{q})\bar{\boldsymbol{L}}(\boldsymbol{q})\big)\boldsymbol{\Phi}^{*}\|_{\infty} \tag{28}$$

and since (25), (26) guarantee that

$$\|I - \boldsymbol{P}(\boldsymbol{q})\bar{\boldsymbol{L}}(\boldsymbol{q})\|_{\infty} < 1 \tag{29}$$

it follows that

$$\|I - \boldsymbol{\Phi P}(\boldsymbol{q})\bar{\boldsymbol{L}}(\boldsymbol{q})\boldsymbol{\Phi}^{*}\|_{\infty} \le \|I - \boldsymbol{P}(\boldsymbol{q})\bar{\boldsymbol{L}}(\boldsymbol{q})\|_{\infty} < 1 \tag{30}$$

■

Theorem 1 and 2 enable a broad class of existing RC schemes to be extended to point-to-point. This is now exemplified through application to the special case of the gradient RC update, proposed in [12], [13] and given by:

Lemma 1: The gradient algorithm is given by

$$\bar{L}(q) = \beta P^{*}(q) \tag{31}$$

where β is a scalar satisfying

$$0 < \beta < \frac{2}{\sup_{\omega\in[0,\pi]} |P(e^{j\omega})|^2} \tag{32}$$

satisfies the traditional RC condition (25), (8). For implementational feasibility, it is necessary that the plant impulse response is less than N samples, i.e. it satisfies

$$C_P A_P^i B_P = 0 \quad \forall \quad i \ge N \tag{33}$$

Using Theorem 1, Theorem 2 and Lemma 1, substitute $\bar{\boldsymbol{L}}(\boldsymbol{q}) = \beta \boldsymbol{P}^{*}(\boldsymbol{q})$ into (23) and (27) to arrive at lifted action

$$\begin{aligned}\boldsymbol{u}(k+1) &= \boldsymbol{u}(k) + \beta \boldsymbol{P}^{*}(\boldsymbol{q})\boldsymbol{\Phi}^{*}\boldsymbol{e}^{\Phi}(k) \\ &= \boldsymbol{u}(k) + \beta\big(\boldsymbol{\Phi P}(\boldsymbol{q})\big)^{*}\boldsymbol{e}^{\Phi}(k)\end{aligned} \tag{34}$$

However, the lifted framework does not admit transparent realisation. Therefore implementation requires conversion to along-the-trial form, as follows.

Proposition 1: Update (34) has equivalent unlifted form

$$\begin{aligned}u((K+1)N+i) =& u(kN+i) + \\ &\beta\Big(\sum_{j=1}^{\bar{i}} CA^{i-i_j}Be((k+1)N+i_j) + \\ &\sum_{j=\bar{i}+1}^{M} CA^{N+i_j-i}Be(kN+i_j)\Big)\end{aligned} \tag{35}$$

where $\bar{i} = \max_j i_j \le i$ defines the most recent point-to-point index with respect to time instant i.

Proof: Consider the required structure of $\boldsymbol{v} = \big(\boldsymbol{\Phi P}(\boldsymbol{q})\big)^{*}\boldsymbol{w}$, i.e.

$$\big(\boldsymbol{\Phi P}(\boldsymbol{q})\big)^{*}: \begin{cases} \boldsymbol{x}_P^{*}(k) = \boldsymbol{A}_P^{\top}\boldsymbol{x}_P^{*}(k+1) + \boldsymbol{C}_P^{\top}\bar{\boldsymbol{\Phi}}^{\top}\boldsymbol{w}(k+1) \\ \qquad\quad = \boldsymbol{A}_P^{\top}\boldsymbol{x}_P^{*}(k+1) + (\bar{\boldsymbol{\Phi}}\boldsymbol{C}_P)^{\top}\boldsymbol{w}(k+1) \\ \boldsymbol{v}(k+1) = \boldsymbol{B}_P^{\top}\boldsymbol{x}_P^{*}(k+1) + \boldsymbol{D}_P^{\top}\bar{\boldsymbol{\Phi}}^{\top}\boldsymbol{w}(k+1) \\ \qquad\quad = \boldsymbol{B}_P^{\top}\boldsymbol{x}_P^{*}(k+1) + (\bar{\boldsymbol{\Phi}}\boldsymbol{D}_P)^{\top}\boldsymbol{w}(k+1) \end{cases} \tag{36}$$

$k \in \mathbb{N}$. Within this there exist the structures

$$(\bar{\boldsymbol{\Phi}}\boldsymbol{C}_P)^{\top} = \big[\, C_P A_P^{i_1}, C_P A_P^{i_2}, \cdots C_P A_P^{i_M} \,\big]^{\top}$$

$$(\bar{\boldsymbol{\Phi}}\boldsymbol{D}_P)^{\top} = \begin{bmatrix} C_P A_P^{i_1} B_P & \cdots & C_P B_P & 0 & \cdots & \cdots & 0 \\ \vdots & \cdots & \ddots & \ddots & & & \vdots \\ C_P A_P^{i_M} B_P & \cdots & \cdots & \cdots & C_P B_P & \underbrace{0 \;\; \cdots \;\; 0}_{N-i_M-1} & \end{bmatrix}^{\top}$$

Now we can write from (36)

$$\boldsymbol{v}(k) = (\bar{\boldsymbol{\Phi}}\boldsymbol{D}_P)^{\top}\bar{\boldsymbol{\Phi}}\boldsymbol{e}(k) + \sum_{i=1}^{\infty}\Big\{\Big(\boldsymbol{C}_P\boldsymbol{A}_P^{i-1}\boldsymbol{B}_P\Big)^{\top}\bar{\boldsymbol{\Phi}}^{\top}\bar{\boldsymbol{\Phi}}\boldsymbol{e}(k+i)\Big\}$$

From (33) it follows that $\boldsymbol{C}_P\boldsymbol{A}_P^{i}\boldsymbol{B}_P = \boldsymbol{0}\ \forall\ i \ge 1$ and hence

$$\boldsymbol{v}(k) = (\bar{\boldsymbol{\Phi}}\boldsymbol{D}_P)^{\top}\bar{\boldsymbol{\Phi}}\boldsymbol{e}(k) + \boldsymbol{B}_P^{\top}(\bar{\boldsymbol{\Phi}}\boldsymbol{C}_P)^{\top}\bar{\boldsymbol{\Phi}}\boldsymbol{e}(k+1) \tag{37}$$

since $\boldsymbol{C}_P\boldsymbol{B}_P =$

$$= \begin{bmatrix} C_P A_P^{N-1} B_P & C_P A_P^{N-2} B_P & \cdots & \cdots & C_P B_P \\ 0 & \ddots & & & \vdots \\ \vdots & \ddots & \ddots & & \vdots \\ \vdots & & \ddots & \ddots & \vdots \\ 0 & \cdots & \cdots & 0 & C_P A_P^{N-1} B_P \end{bmatrix}$$

we have $\boldsymbol{B}_P^\top(\bar{\boldsymbol{\Phi}}\boldsymbol{C}_P)^\top = (\bar{\boldsymbol{\Phi}}\boldsymbol{C}_P\boldsymbol{B}_P)^\top =$

$$\begin{bmatrix} \overbrace{0 \ \cdots \ 0}^{i_1} & C_PA_P^{N-1}B_P & \cdots & \cdots & C_PA_P^{i_1}B_P \\ & \ddots & & \ddots & \vdots \\ \underbrace{0 \qquad \cdots \qquad 0}_{i_M} & C_PA_P^{N-1}B_P & \cdots & & C_PA_P^{i_M}B_P \end{bmatrix}^\top$$

and therefore point-to-point RC update (37) is

$$\boldsymbol{u}(k+1) = \boldsymbol{u}(k) + \beta\times$$
$$\left[\begin{bmatrix} C_PA_P^{i_1}B_P & \cdots & C_PB_P & 0 & \cdots & \cdots & 0 \\ \vdots & \cdots & \ddots & \ddots & & & \vdots \\ C_PA_P^{i_M}B_P & \cdots & \cdots & \cdots & C_PB_P & \underbrace{0 \ \cdots \ 0}_{N-i_M-1} & \end{bmatrix}^\top \times \right.$$
$$\left.\begin{bmatrix} \overbrace{0 \ \cdots \ 0}^{i_1} & C_PA_P^{N-1}B_P & \cdots & \cdots & C_PA_P^{i_1}B_P \\ & \ddots & & \ddots & \vdots \\ \underbrace{0 \qquad \cdots \qquad 0}_{i_M} & C_PA_P^{N-1}B_P & \cdots & & C_PA_P^{i_M}B_P \end{bmatrix}^\top\right]$$
$$\times \begin{bmatrix} \bar{\boldsymbol{\Phi}}\boldsymbol{e}(k) \\ \bar{\boldsymbol{\Phi}}\boldsymbol{e}(k+1) \end{bmatrix} \tag{38}$$

which can be written as the along-the-trial update (35). ■

The next result shows that the point-to-point update (34), (35) converges to a minimum control effort solution.

Theorem 3: Application of point-to-point gradient RC law (34) or (35) to system (1) satisfies the tracking requirement (21) with a control input that converges to the minimum control effort, i.e. satisfies (22) with

$$\hat{\boldsymbol{u}} := \min_{\boldsymbol{u}} \|\boldsymbol{u}\|^2 \quad \text{such that} \quad \boldsymbol{r}^\Phi = \boldsymbol{\Phi}\boldsymbol{P}\hat{\boldsymbol{u}} \tag{39}$$

Proof: From (13) the steady-state solution satisfies:

$$\boldsymbol{y}(k+1) = \boldsymbol{D}_P\boldsymbol{u}(k+1) + \boldsymbol{C}_P\boldsymbol{B}_P\boldsymbol{u}(k) \tag{40}$$

where $\boldsymbol{u}(k) = \hat{\boldsymbol{u}} \ \ \forall k$. Hence

$$\boldsymbol{y}(k) = \big(\boldsymbol{D}_P + \boldsymbol{C}_P\boldsymbol{B}_P\big)\hat{\boldsymbol{u}} \quad \forall k \tag{41}$$

and

$$\bar{\boldsymbol{\Phi}}\boldsymbol{y}(k) = \bar{\boldsymbol{\Phi}}\big(\boldsymbol{D}_P + \boldsymbol{C}_P\boldsymbol{B}_P\big)\hat{\boldsymbol{u}} \quad \forall k \tag{42}$$

The solution to (39) is then

$$\hat{\boldsymbol{u}} = \big(\bar{\boldsymbol{\Phi}}\big(\boldsymbol{D}_P + \boldsymbol{C}_P\boldsymbol{B}_P\big)\big)^\dagger \boldsymbol{r}^\Phi \tag{43}$$

where $A^\dagger := A^\top\big(AA^\top\big)^{-1}$. Consider the lifted point-to-point gradient implementation, given by $\boldsymbol{u}(k+1) =$

$$\boldsymbol{u}(k) + \beta(\bar{\boldsymbol{\Phi}}\boldsymbol{D}_P)^\top\bar{\boldsymbol{\Phi}}\boldsymbol{e}(k) + \beta(\bar{\boldsymbol{\Phi}}\boldsymbol{C}_P\boldsymbol{B}_P)^\top\bar{\boldsymbol{\Phi}}\boldsymbol{e}(k+1)$$
$$= \boldsymbol{u}(k) + \beta\big(\bar{\boldsymbol{\Phi}}\big(\boldsymbol{D}_P + \boldsymbol{C}_P\boldsymbol{B}_P\big)\big)^\top\boldsymbol{r}^\Phi - \beta\big((\bar{\boldsymbol{\Phi}}\boldsymbol{D}_P)^\top\bar{\boldsymbol{\Phi}}\boldsymbol{D}_P +$$
$$(\bar{\boldsymbol{\Phi}}\boldsymbol{C}_P\boldsymbol{B}_P)^\top\bar{\boldsymbol{\Phi}}\boldsymbol{C}_P\boldsymbol{B}_P\big)\boldsymbol{u}(k) - \beta(\bar{\boldsymbol{\Phi}}\boldsymbol{D}_P)^\top\bar{\boldsymbol{\Phi}}\boldsymbol{C}_P\boldsymbol{B}_P\boldsymbol{u}(k-1)$$
$$- \beta(\bar{\boldsymbol{\Phi}}\boldsymbol{C}_P\boldsymbol{B}_P)^\top\bar{\boldsymbol{\Phi}}\boldsymbol{D}_P\boldsymbol{u}(k+1)$$

Hence

$$\boldsymbol{u}(k+1) = \Big[I + \beta(\bar{\boldsymbol{\Phi}}\boldsymbol{C}_P\boldsymbol{B}_P)^\top\bar{\boldsymbol{\Phi}}\boldsymbol{D}_P\Big]^{-1}\times$$
$$\Big\{\beta\big(\bar{\boldsymbol{\Phi}}\big(\boldsymbol{D}_P + \boldsymbol{C}_P\boldsymbol{B}_P\big)\big)^\top\boldsymbol{r}^\Phi - \beta(\bar{\boldsymbol{\Phi}}\boldsymbol{D}_P)^\top\bar{\boldsymbol{\Phi}}\boldsymbol{C}_P\boldsymbol{B}_P\boldsymbol{u}(k-1)$$
$$+ \Big[I - \beta\big((\bar{\boldsymbol{\Phi}}\boldsymbol{D}_P)^\top\bar{\boldsymbol{\Phi}}\boldsymbol{D}_P + (\bar{\boldsymbol{\Phi}}\boldsymbol{C}_P\boldsymbol{B}_P)^\top\bar{\boldsymbol{\Phi}}\boldsymbol{C}_P\boldsymbol{B}_P\big)\Big]\boldsymbol{u}(k)\Big\} \tag{44}$$

This has the form

$$\boldsymbol{u}(k+1) = a\boldsymbol{u}(k) + b\boldsymbol{u}(k-1) + c \tag{45}$$

and writing

$$\begin{bmatrix} \boldsymbol{u}(k+1) \\ \boldsymbol{u}(k+2) \end{bmatrix} = \underbrace{\begin{bmatrix} b & a \\ ab & a^2+b \end{bmatrix}}_{\Xi}\begin{bmatrix} \boldsymbol{u}(k-1) \\ \boldsymbol{u}(k) \end{bmatrix} + \underbrace{\begin{bmatrix} c \\ ac+c \end{bmatrix}}_{\Theta}$$

with, if $\rho(\Xi) < 1$, we use block matrix inverse relations, see, e.g. [14], to write after extensive manipulations

$$\begin{bmatrix} \boldsymbol{u}(\infty) \\ \boldsymbol{u}(\infty) \end{bmatrix} = \sum_{i=1}^{\infty}\Xi^i\Theta = (I-\Xi)^{-1}\Theta \quad = \begin{bmatrix} (I-b-a)^{-1}c \\ (I-b-a)^{-1}c \end{bmatrix} \tag{46}$$

From (44) and (45), it follows that $(I-a-b)^{-1}c$ equals

$$\Big\{(\bar{\boldsymbol{\Phi}}\boldsymbol{D}_P)^\top\bar{\boldsymbol{\Phi}}\boldsymbol{D}_P + (\bar{\boldsymbol{\Phi}}\boldsymbol{C}_P\boldsymbol{B}_P)^\top\bar{\boldsymbol{\Phi}}\boldsymbol{C}_P\boldsymbol{B}_P + (\bar{\boldsymbol{\Phi}}\boldsymbol{D}_P)^\top\bar{\boldsymbol{\Phi}}\boldsymbol{C}_P\boldsymbol{B}_P$$
$$+ (\bar{\boldsymbol{\Phi}}\boldsymbol{C}_P\boldsymbol{B}_P)^\top\bar{\boldsymbol{\Phi}}\boldsymbol{D}_P\Big\}^{-1}\big(\bar{\boldsymbol{\Phi}}\big(\boldsymbol{D}_P + \boldsymbol{C}_P\boldsymbol{B}_P\big)\big)^\top\boldsymbol{r}^\Phi =$$
$$\Big\{\big(\bar{\boldsymbol{\Phi}}\big(\boldsymbol{D}_P + \boldsymbol{C}_P\boldsymbol{B}_P\big)\big)^\top\bar{\boldsymbol{\Phi}}\big(\boldsymbol{D}_P + \boldsymbol{C}_P\boldsymbol{B}_P\big)\Big\}^{-1}\big(\bar{\boldsymbol{\Phi}}\big(\boldsymbol{D}_P +$$
$$\boldsymbol{C}_P\boldsymbol{B}_P\big)\big)^\top\boldsymbol{r}^\Phi = \big(\bar{\boldsymbol{\Phi}}\big(\boldsymbol{D}_P + \boldsymbol{C}_P\boldsymbol{B}_P\big)\big)^\dagger\boldsymbol{r}^\Phi \tag{47}$$

as required. ■

IV. Stimulated Ankle Dynamics

Application of FES to Drop-Foot is typically achieved using transutaneous surface electrodes placed near the peroneal nerve in order to generate natural foot lift via activation of the patient's shank muscles. The only model-based FES controller that currently exists for Drop-Foot trajectory tracking is reported in [8], and identified the electrically-stimulated dynamics as a third order discrete transfer function via black box least-squares fitting. To embed greater transparency, a parametrised model is now developed to enable model-based design and simulation.

The ankle is a complex structure and a wide range of models have been proposed to capture underlying kinematic and kinetic properties. Depending on the application, complexity is reduced by grouping or omitting ligaments, and assuming isotropic, homogenous properties to muscle and cartilage [15]. Similarly, tendons are typically modelled as tension-only elastic strings, bones are treated as rigid bodies and effects caused by soft tissues are ignored [16]. Accordingly, here we assume rigid body dorsiflexion/plantarflexion dynamics [17] with parameters extracted from the experimental motion and EMG data in [18] and [19] using linear regression. This is combined with a Hill type model of muscle dynamics [20] which characterises both voluntary and artificial muscle activation. Here torque

is modelled as the product of a force-length property, and a nonlinear muscle activation dynamics under isometric conditions, which are represented by a static nonlinearity in series with linear activation dynamics [21]. The resulting muscle dynamics are validated in [22] and in the current case experimental parameters are taken from [23] and [24].

A sampling time of 50 Hz is selected and the combined forth-order model is represented in form (1) with input FES pulsewidth (μs), and output dorsiflexion angle (degrees).

A. Gait Cycle

A typical unimpaired human gait cycle is shown in Fig. 3, and has been computed by amalgamating experimental results from [25] and [26] The gait cycle is commonly split into stance (60% of motion) and swing (40 % of motion) phases, with the whole motion often further partitioned into 8 distinct sections [27]. The key features in stance include; heel strike, flat foot, midstance, heel-off, toe-off which marks the end of stance and beginning of swing, acceleration, mid-swing and finally deceleration before heel strike occurs again. The timing of these key features has been added to the figure. The period of each cycle varies significantly, but an average of 2 s is often assumed.

V. Application of Point-to-Point to Drop-Foot

Having established the stimulated ankle dynamics and gait profile, the proposed point-to-point RC is applied and compared with standard RC. To do this it is necessary to extract the time instances $i_1 \cdots i_M$ and corresponding positions $r(i_1) \cdots r(i_M)$ used by the former algorithm. Here M should be the minimum number necessary to characterise normal gait motion. From Fig. 3, the critical $(\%Gaitcycle, r(i_j))$ points are: flat foot $(9, 0°)$, heel off $(44, 12°)$, toe off $(63.55, -14.5°)$ and start of mid swing $(78, 1.629°)$. From the period and sampling frequency it follows that $N = 100$.

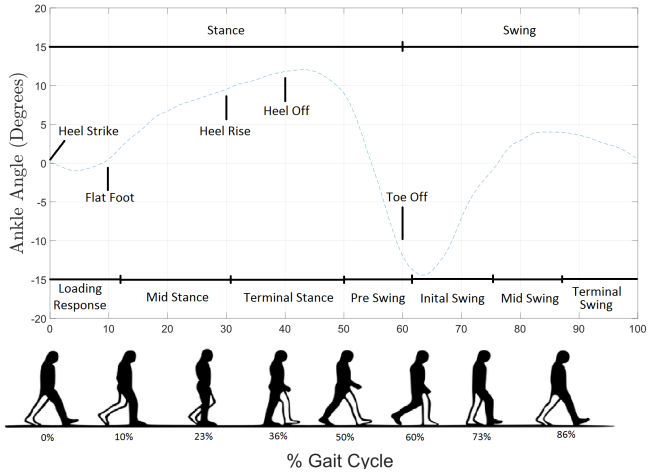

Fig. 3. Standardised Gait Cycle, with gait events/phases labled.

A. Nominal Performance Comparison

First, standard RC is applied with reference r set to the full profile shown in Fig 3. Update 35 is applied using $M = N = 100$, $i_1 = 1, i_2 = 2, \cdots, i_M = 100$. A range of β are applied to establish maximum convergence, as can be seen in Fig. 4. Whilst using the optimum value of $\beta = 2.7$, the error norm $||e||$ is slow, requiring 10321 cycles to reduce the error norm convergence below 1% of its initial value. Faster convergence is not possible since divergence occurs with larger β. Next point-to-point RC is applied using

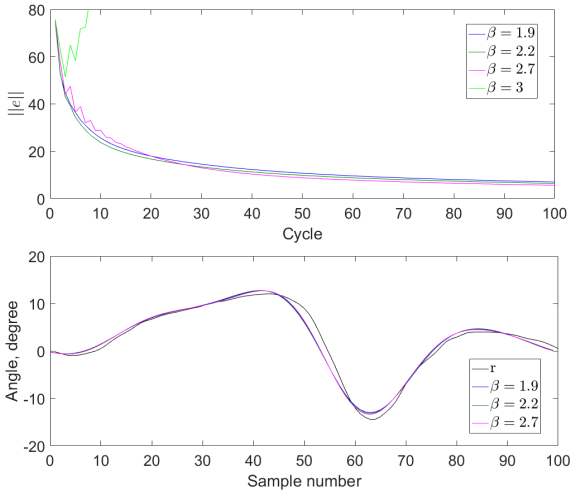

Fig. 4. Standard RC, convergence and final gait output.

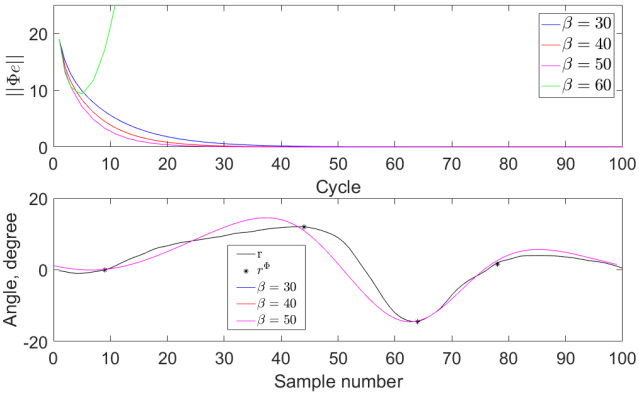

Fig. 5. Point-to-Point RC, signal output, convergence and final gait output.

$M = 4$ and the set $\{i_j\}$ defined in Section V. Using the optimal β value, the error norm $||\Phi e||$ falls below 1% of its initial value after 16 cycles.

Output behaviour between points is smooth, as expected by the minimum control effort property of Theorem 3. The correspondence between limiting output y and full gait r also reflects results from human motor control that natural motion can be posed as a minimum effort problem. This indicates that point-to-point RC assists motion in a natural manner.

B. Affect of Model Uncertainty

To investigate the affect of model uncertainty in standard and point-to-point RC, a 40% uncertainty has been applied across two variables in the model; stiffness and damping.

The best β values used previously are reduced to 80% of their original value. The results are shown in Fig 6.

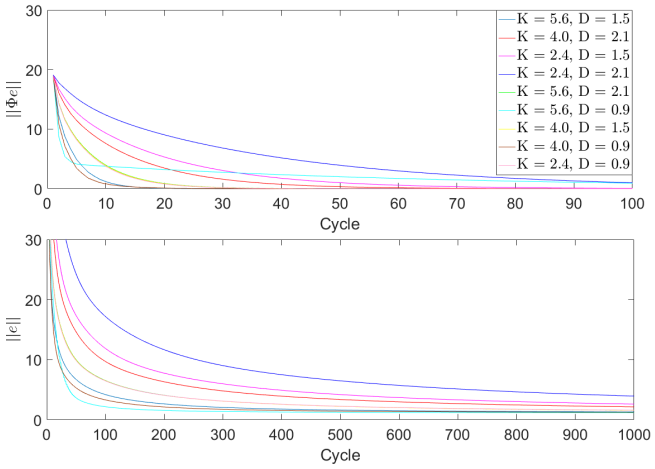

Fig. 6. Convergence rate: Point-to-point RC (Top); Standard RC (Bottom)

For the biggest uncertainty, an increase in stiffness by 40% and decrease in damping by 40%, the standard RC error norm ($||e||$) falls below 1% of its initial value in 2967 cycles, using a value of $\beta = 2.16$. In contrast, the error norm in point-to-point RC $||\Phi e||$ falls below 1% of its initial value in 95 cycles, using $\beta = 40$. Demonstrating a faster convergence for the point-to-point controller.

VI. Conclusion

This paper proposes a new form of RC which provides convergence at specific time points, thereby reducing computational load and increasing flexibility. The framework permits a wide class of algorithm to be designed. It goes on to apply the framework to Drop-Foot where it improves on existing approaches by offering precise tracking with the advantage of requiring minimal sensor data or computation. In particular, point-to-point RC provides two orders of magnitude faster convergence than standard RC. Additionally, point-to-point RC demonstrated faster convergence despite uncertainty within the model, indicating that point-to-point RC is more robust to model error. These results establish the potential of point-to-point RC for Drop-Foot, and more generally in related applications such as knee control, sit-to-stand, cycling, rowing and other common stroke rehabilitation exercises.

APPENDIX

This work was supported by Engineering and Physical Sciences Research Council grant EP/M026388/1.

References

[1] C. L. Barrett and P. N. Taylor. The effects of the odstock drop foot stimulator on perceived quality of life for people with stroke and multiple sclerosis. *Neuromodulation*, 13(1):58–64, 2010.

[2] E. W. Peterson. Fear of falling and associated activity curtailing among middle aged and older adults with multiple scleosis. *Mult Scler*, 13:1168–1175, 2007.

[3] J. E. Esnouf et al. Impact on activities of daily living using a functional electrical stimulation device to improve dropped foot in people with multiple sclerosis, measured by the canadian occupational performance measure. *Mult Scler*, 16:1141–1147, 2010. Taylor, P. N. and Mann, G. E. and Barrett, C. L.

[4] A. Roche, G. O. Laighin, and S. Coote. Surface-applied functional electrical stimulation for orthotic and therapeutic treatment of drop-foot after stroke: a systematic review. *Phys. Ther. Rev.*, 14(2), 2009.

[5] D. N. Rushton. Functional electrical stimulation and rehabilitation - an hypothesis. *Medical Engineering and Physics*, 25(1):75–78, 2003.

[6] N. Negrd. *Controlled FES-assisted gait training for hemiplegic stroke patients based on inertial sensors*. PhD thesis, TU Berlin, 2009.

[7] N. Mourselas and M. Granat. Correction of drop foot using a fuzzy logic controlled miniature stimulator. In *5th conf. int. funct. elect. stim. soc.*, pages 140–141, 2000.

[8] T. Seel, C. Werner, J. Raisch, and T.Schauer. Iterative learning control of a drop foot neuroprosthesis generating physiological foot motion in paretic gait by automatic feedback control. *Control Engineering Practice*, 48(3):87–97, 2016.

[9] L. Wang, S. Chai, E. Rogers, and C. T. Freeman. Multivariable repetitivepredictive controllers using frequency decomposition. *IEEE Transactions on Control System Technology*, 20(6):1597–1604, 2012.

[10] C. T. Freeman and Y. Tan. Iterative learning control with mixed constraints for point-to-point tracking. *IEEE Transactions on Control System Technology*, 21(3):604–616, 2013.

[11] G. Pipeleers and K. L. Moore. Unified analysis of iterative learning and repetitive controllers in trial domain. *IEEE Transactions on Automatic Control*, 59(4):953–965, 2014.

[12] J. J. Hätönen, C. T. Freeman, D. H. Owens, P. L. Lewin, and E. Rogers. A gradient-based repetitive control algorithm combining ILC and pole placement. *Euro. J. of Control*, 12(3):278–292, 2006.

[13] J. J. Hätönen, C. T. Freeman, D. H. Owens, P. L. Lewin, and E. Rogers. Robustness analysis of a gradient-based repetitive algorithm for discrete-time systems. In *Proc. of the 43th Conf. on Decision and Control*, pages 1301–1306, 2004.

[14] T-T. Lu and S-H. Shiou. Inverses of 2 x 2 block matrices. *Computers and Mathematics with Applications*, 43:119–129, 2002.

[15] M. H. Ramlee, M. R. A. Kadir, and H. Harun. Three-dimensional modeling and analysis of a human ankle joint. In *IEEE Student Conference on Research and Developement*, pages 74–78, 2013.

[16] Z. Fenfang, G. Zhu, Y. H. Tsoi, and S. Xie. A computational biomechanical model of the human ankle for development of an ankle rehabilitation robot. In *IEEE/ASME 10th Int.l Conf. Mechatronic and Embedded Systems and Applications*, pages 1–6, 2014.

[17] M. Lin L. Q. Zhang, D. Makhsous. Stiffness and viscous damping of the human leg. *American Society of Biomechanics*, 2000. Chicago.

[18] M Munih, K Hunt, and N Donaldson. Variation of recruitment nonlinearity and dynamic response of ankle plantarflexors. *Medical Engineering and Physics*, 22(2):97 – 107, 2000.

[19] L. Mesin, E. Merlo, R. Merletti, and C. Orizio. Investigation of motor unit recruitment during stimulated contractions of tibialis anterior muscle. *J. of Electromyogr.and Kinesiol.*, 20(4):580 – 589, 2010.

[20] L. Sun, Y. Sun, Z. Huang, J. Hou, and J. Wu. A hill-type submaximally-activated musculotendon model and its simulation. In *14th Int. Symp. on Distributed Comp.and Applicat. for Business Eng. and Sci.*, pages 439–442, 2015.

[21] A. Assalone, G. Pin, and T. Parisini. Kernel-based continuous-time identification of hammerstein models: Application to the case of ankle joint stiffness dynamics. In *IEEE International Conference on Rehabilitation Robotics*, pages 2015–2020, 2015.

[22] F. Le, I. Markovsky, C. T. Freeman, and E. Rogers. Identification of the dynamics of human arms after stroke. In *Proc. 23rd IAR Workshop Adv. Cont. Diag.*, 2008.

[23] E. J. Rouse et al. The difference between stiffness and quasi-stiffness in the context of biomechanical modeling. *IEEE Trans. Biomed. Eng.*, pages 562–568, 2013. R. D. Gregg and L. J. Hargrove and J. W. Sensinger.

[24] E. M. Ficanha, G. A. Ribeiro, L. Knop, and M. Rastgaar. Time-varying impedance of the human ankle in the sagittal and frontal planes during straight walk and turning steps. In *Int. Conf. Rehab. Rob.*, pages 1413–1418, July 2017.

[25] N. Postans and M. Granat. Effect of functional electrical stimulation, applied during walking, on gait in spastic cerebral palsy. *Developmental Medicine and Child Neurology*, 47(1):46–52, 2005.

[26] R. Neptune and K. Sasaki. Ankle plantar flexor force production is an important determinant of the preferred walk-to-run transition speed. *Journal of Experimental Biology*, 208(5):799–808, 2005.

[27] H. Zhang, J. Qian, L. Shen, and Y. Zhang. Research on healthy subject gait cycle phase at different walking speeds. In *IEEE Int. Conf. Rob. Biomimet.*, pages 1349–1354, 2012.